Autism candidate gene *rbm-26* (*RBM26/27*) regulates MALSU-1 to protect against mitochondrial dysfunction during axon development.

Tamjid A Chowdhury[1], David A Luy[1], Dorian Farache[2,3], Amy SY Lee[2,3], Christopher C Quinn[1*]

[1] Department of Biological Sciences, University of Wisconsin-Milwaukee, Milwaukee, WI, USA.
[2] Department of Cell Biology, Harvard Medical School, Boston, MA, USA.
[3] Department of Cancer Immunology and Virology, Dana-Farber Cancer Institute, Boston, MA, USA.

[*]To whom correspondence should be addressed at: Department Biological Sciences
3209 N. Maryland Avenue
Milwaukee, WI 53211

EMAIL: quinnc@uwm.edu
Phone: (414)229-2602
Fax: (414)229-3926

Abstract

Mitochondrial dysfunction is thought to be a key component of neurodevelopmental disorders such as autism, intellectual disability, and ADHD. However, little is known about the molecular mechanisms that protect against mitochondrial dysfunction during neurodevelopment. Here, we address this question through the investigation of *rbm-26*, the *C. elegans* ortholog of the *RBM27* autism candidate gene, which encodes an RNA-binding protein whose role in neurons is unknown. We report that RBM-26 (RBM26/27) protects against neurodevelopmental defects by negatively regulating expression of the MALSU-1 mitoribosomal assembly factor. Autism-associated missense variants in RBM-26 cause a sharp decrease in RBM-26 protein expression along with neurodevelopmental defects, including errors in axon targeting and axon degeneration. Using an unbiased screen, we identified the mRNA for the MALSU-1 mitoribosomal assembly factor as a binding partner for RBM-26. RBM-26 negatively regulates the expression of *malsu-1* mRNA and MALSU-1 protein, and genetic analysis indicates that this interaction is required to protect against neurodevelopmental defects. Moreover, biochemical evidence suggests that excess levels of MALSU-1 disrupt the biogenesis of mitoribosomes in *rbm-26* mutants. These observations reveal a mechanism that can protect mitochochondrial function to prevent neurodevelopmental defects and suggest that disruptions in this process can cause neurodevelopmental disorders.

Introduction

Emerging evidence suggests an association between mitochondria and neurodevelopmental disorders including autism, intellectual disability, and attention deficit hyperactivity disorder (ADHD). For example, certain mitochondrial DNA lineages confer substantial risk for autism and ADHD [1, 2]. Likewise, heteroplasmic mtDNA mutations are also a risk factor for autism and intellectual disability [3-5]. Consistent with a causative role for mitochondria dysfunction in neurodevelopmental disorders, mice with a hypomorphic missense mutation in the *ND6* mtDNA gene exhibit autism endophenotypes and also produce excess ROS in the brain [6]. In this regard, it is intriguing to note that elevated levels of reactive oxygen species (ROS) have also been observed in autistic human brains [7]. Together, these observations suggest that mitochondrial dysfunction plays a causative role in neurodevelopmental disorders. However, little is known about the mechanisms that protect mitochondria function during neurodevelopment.

Consistent with a role for mitochondria in neurodevelopmental disorders, some of these disorders include a neurodegenerative phenotype. For example, loss of *EXOSC3* or *EXOSC9* gene function causes a neurodevelopmental syndrome that includes intellectual disability and axon degeneration [12-14]. Likewise, loss of the *GAN* gene in humans causes the giant axonal neuropathy disease, featuring axon degeneration and intellectual disability in children [15]. Moreover, loss of either the *SPTBN1* or *ADD1*

genes causes a neurodevelopmental syndrome that includes autism and ADHD. In mouse models, variants in these genes cause defects in axon targeting along with axon degeneration, suggesting that these phenotypes may be a cause for the human syndrome [8-11]. Together, these observations suggest that neurodegeneration may contribute to at least some neurodevelopmental disorders. However, little is known about the cellular and molecular mechanisms that protect against neurodegeneration during neurodevelopment.

The *RBM27* (*rbm-26*/*Swm*/*Rmn1*) gene encodes an RNA binding protein and is considered an autism candidate gene by the Simmons Foundation Autism Research Initiative (SFARI) [16]. In a cultured human cell line, RBM27 and its paralog RBM26 can function with the PAXT connection, an adaptor complex for the nuclear RNA exosome [17]. Likewise, in *S. pombe* the Rmn1 ortholog of RBM26/27 can also function as part of an adaptor for the nuclear RNA exosome [18]. In *Drosophila,* the Swm ortholog of RBM26/27 has also been implicated in RNA metabolism and the maintenance of adult intestinal stem cells [19]. Despite these findings, the role of RBM27 and its orthologs in neurons have not been investigated. Moreover, the identity of *RBM27* as an autism candidate gene is based on de novo missense mutations that have not been tested for gene-disrupting activity.

Here, we identify a mitochondria-protecting role for the RBM-26 ortholog of RBM26/27 that prevents axon degeneration and axon targeting defects during development. We find that loss of RBM-26 function causes mitochondrial dysfunction in the developing neuron along with axon beading and defects in axon targeting. These phenotypes are induced by an *rbm-26* null allele as well as by alleles that are equivalent to autism-associated de novo missense variants in *RBM27*, suggesting that these missense mutations disrupt gene function. Mechanistically, we identified the *malsu-1* mRNA as a binding partner for RBM-26 and found that RBM-26 negatively regulates the expression of the *malsu-1* mRNA, which encodes a mitoribosomal assembly factor. Moreover, analysis of gain-of-function and loss-of function experiments indicate that MALSU-1 is required for both the axon degeneration phenotype and the mitochondrial phenotypes that are caused by loss of RBM-26. Consistent with a defect in mitoribosomal assembly, we also find that loss of RBM-26 function causes a sharp reduction in mitoribosomes. These observations indicate that RBM-26 negatively regulates MALSU-1 expression to protect against mitochondrial dysfunction and defects in axon development.

Results

Expression of RBM-26 is disrupted by P80L and L13V missense mutations.

RBM27 has been identified as a candidate autism gene by the Simons Foundation Autism Research Initiative (SFARI) [16]. The potential association of *RBM27* with autism is based on the identification of 5 de novo variants in probands with autism or

intellectual disability, but none in unaffected siblings (Fig. 1A). However, the confidence in this association is limited by the fact that the identified variants are all missense variants, rather than likely-gene-disrupting variants. Moreover, a role for *RBM27* in neurodevelopment has not been investigated. To address these issues, we used the *C. elegans rbm-26* ortholog of *RBM27.* We found that 2 of the 5 de novo missense mutation sites in human RBM27 are conserved in *C. elegans rbm-26*. These two conserved missense mutations cause L13V and P79L amino acid changes in human RBM27, which are equivalent to L13V and P80L respectively in *C. elegans* RBM-26 (Fig. 1B).

To determine how the L13V and P80L variants affect RBM-26 protein expression, we used CRISPR to introduce these mutations into the endogenous *rbm-26* gene and also added a 3XFLAG tag to allow for detection by western blot. A sequence encoding 3XFLAG was inserted just upstream of the *rbm-26* stop codon, thereby creating the *rbm-26(cue25)* allele, hereafter referred to as *rbm-26(3XFLAG)*. Next, we used CRISPR to introduce the P80L mutation into the *rbm-26(3XFLAG)* allele, thereby creating the *rbm-26(cue22)* allele, hereafter called *rbm-26(P80L::3XFLAG)*. We also used CRISPR to introduce the L13V mutation into the *rbm-26(3XFLAG)* allele, thereby creating the *rbm-26(cue24)* allele, hereafter called *rbm-26(L13V::3XFLAG)*.

We next used western blotting to detect the RBM-26::3XFLAG, RBM-26 P80L::3XFLAG, and RBM-26 L13V::3XFLAG proteins. The wild-type *rbm-26* gene is predicted to produce RBM-26 proteins with molecular weights around 72 and 79 KD. Consistent with this prediction, we found that the RBM-26::3XFLAG protein was detected as a band just above the 72KD marker. In addition, we also observed a band at around 56 KD. The identity of this 56 KD band is unknown, though it is likely an unpredicted splice form or the result of post-translational processing. We also found that the RBM-26 P80L::3XFLAG and RBM-26 L13V::3XFLAG proteins were expressed at much lower levels relative to wild-type RBM-26::3XFLAG (Fig. 3C). Taken together, these results suggest that the P80L and L13V mutations cause a sharp decrease in expression of RBM-26.

Mutations in *rbm-26* cause axon degeneration and defects in axon targeting.

For these studies, we focused on the PLM, a neuron that has its cell body in the tail and extends an axon anteriorly along the lateral body wall (Fig. 2A-B) Nearly all wild-type PLM axons terminate prior to reaching the ALM cell body (Fig. 2A,B,D). To determine how loss of RBM-26 function affects the PLM, we used the *rbm-26(gk910)* null mutation, hereafter called *rbm-26(null)*. This *rbm-26(null)* allele consists of a 408 base pair deletion that removes part of exon 4 and exon 5 of *rbm-26* and is lethal. We maintained the *rbm-26(null)* allele over a balancer and found that maternally rescued homozygote progeny are viable until the L3 stage. Therefore, we analyzed the PLM axon in maternally rescued L3 stage *rbm-26(null)* homozygotes. We found that in *rbm-26(null)*

mutants, the PLM failed to terminate prior to reaching the ALM cell body with a penetrance of about 40% (Fig 2C,D). Moreover, in about 30% of *rbm-26(null)* mutant PLM axons we also observed an axon beading phenotype (Fig 2E,F). This axon beading phenotype has previously been reported in aging worms [20-22] and is reminiscent of axonopathy that has been reported in human neurodegenerative disorders and described as axonal swellings or spheroids [23-25]. Overall, these observations suggest that RBM-26 promotes PLM axon termination and protects against axon degeneration.

To address the function of the RBM-26 P80L and RBM-26 L13V mutant proteins, we used CRISPR to add these missense mutations to the *rbm-26* gene. We introduced the P80L missense mutation into the *rbm-26* gene, creating the *rbm-26(cue23)* mutation, hereafter referred to as *rbm-26(P80L)*. We also introduced the L13V missense mutation into the *rbm-26* gene, creating the *rbm-26(cue34)* mutation, hereafter referred to as *rbm-26(L13V)*. In contrast to the *rbm-26(null)* mutation, both the *rbm-26(P80L)* and the *rbm-26(L13V)* mutations were viable. Moreover, we found that both of these mutations cause axon termination defects, albeit at a lower penetrance relative to the *rbm-26(null)* mutation (Fig. 2D). In addition, both of these mutations also cause axon beading (Fig. 2F). These results imply that the P79L and L13V de novo missense mutations in human *RBM27* are likely to disrupt *RBM27* function, thereby supporting a role for this gene in autism and intellectual disability.

RBM-26 is expressed in multiple tissues and functions within neurons to protect against neurodegeneration and prevent defects in axon targeting.

To visualize the localization of RBM-26, we used CRISPR to insert the coding sequence for a SCARLET::AID (auxin-inducible degron) tag into the 3′ end of the *rbm-26* gene, thereby creating the *rbm-26(*syb2552) allele. We found that this allele expresses RBM-26::SCARLET::AID in many tissues including neurons, hypodermis, muscle, and intestine. Within hypodermis and neurons, we noticed that the RBM-26::SCARLET::AID protein was localized to the nucleus (Fig. 3A,B,D).

We next asked where RBM-26 functions to protect against axon degeneration and targeting defects. To address this question, we used the auxin-inducible degron system to selectively degrade the RBM-26::SCARLET::AID protein in in neurons, hypodermis, muscle, and intestine. We found that degradation of RBM-26::SCARLET::AID in neurons caused both PLM axon termination defects (Fig. 3E) and the PLM axon beading phenotype (Fig. 3F). However, degradation of RBM-26::SCARLET::AID in hypodermis, muscle, or intestine failed to cause any of these phenotypes (Figures 3E-F). These observations suggest that RBM-26 is broadly expressed and that it functions cell-autonomously within neuronal nuclei to protect against axon degeneration and axon targeting defects.

Loss of RBM-26 causes mitochondria dysfunction in axons.

Mitochondrial dysfunction is thought to be an early causative factor for axon degeneration. Therefore, we asked if loss of RBM-26 function affects mitochondria in axons. We found that mitochondria were localized throughout wild-type PLM axons, with an average of about 21 mitochondria per axon (Fig. 4A,B,E). The *rbm-26(null)* mutation caused a reduction of the average number of mitochondria to about 12 per PLM axon (Fig. 4C-E). The *rbm-26(P80L)* and the *rbm-26(L13V)* mutations caused a less severe reduction in the average number of mitochondria per PLM axon (Fig. 4E). These observations suggest that RBM-26 is needed to maintain a normal number of mitochondria in the axon.

Excess production of reactive oxidation species (ROS) is a key marker for mitochondrial dysfunction[26, 27]. Therefore, we asked if the *rbm-26(null)* mutation causes an increase in ROS production by mitochondria. For this experiment, we used mitoTimer, an oxidation sensor that is tethered to mitochondria and changes irreversibly from green to red as it becomes oxidized [28]. We found that the *rbm-26(P80L)* mutation significantly increased the mitoTImer red:green ratio (Fig. 4F-H), suggesting that this mutation causes mitochondria to produce excessive ROS. We also tested the *rbm-26(null)* mutation and found that it also increased the mitoTImer red:green ratio (Fig. 4I). These observations suggest that loss of *rbm-26* function causes mitochondrial dysfunction.

RBM-26 binds to the *malsu-1* mRNA and negatively regulates its expression.

To understand the molecular mechanisms of RBM-26 function in axon targeting and degeneration, we conducted a screen to identify RNAs that bind to RBM-26. For this screen, we used ultraviolet light to induce RNA-protein crosslinking in strains expressing RBM-26::3XFLAG and in controls expressing GFP::3XFLAG and SCARLET::3XFLAG (see methods for details). We than used an anti-FLAG antibody to purify the RBM-26::3XFLAG::RNA and SCARLET/GFP::3XFLAG::RNA complexes, followed by RNA-Seq analysis. We identified 63 RNAs that were significantly enriched in RBM-26::3XFLAG pulldowns relative to SCARLET/GFP::3XFLAG controls (Figure 5A). Among these 63 RNAs we found 26 protein-coding mRNAs, 14 non-coding RNAs, 8 piRNAs, and 10 snoRNAs, 1 tRNA and 1rRNA (Supplemental Table 1).

Considering the RNA binding partners for RBM-26, we focused on the *malsu-1* mRNA because it encodes an ortholog of the mammalian MALSU1 mitochondrial ribosome assembly factor [29]. Using qPCR, we found that loss of RBM-26 function causes an increase in *malsu-1* mRNA expression in *rbm-26(P80L)* mutants relative to wildtype (Fig. 5B). To analyze MALSU-1 protein expression, we used CRISPR to add a 3XFLAG tag to MALSU-1, thereby creating the *malsu-1(cue37)* allele, which expresses the MALSU-1::3XFLAG protein. Since the *malsu-1* gene is tightly linked to the *rbm-26* gene,

we used CRISPR to introduce the P80L mutation into a strain containing the *malsu-1(cue37)* mutation, thus creating the *malsu-1(cue37); rbm-26(cue42 [P80L])* double mutant. By performing western blotting to analyze expression of MALSU-1::3XFLAG in these strains we found that loss of RBM-26 function substantially enhances expression of the MALSU-1::3XFLAG protein relative to wild type (Fig. 5C). These observations indicate that RBM-26 negatively regulates the expression of *malsu-1* mRNA and MALSU-1 protein.

Overexpression of MALSU-1 reduces mitochondria in the PLM axon and causes axon degeneration and defects in axon targeting.

Since we found that loss of RBM-26 function causes an increase in MALSU-1 expression, we next asked if this overexpression of MALSU-1 could account for the axonal phenotypes of *rbm-26* mutants. For this experiment, we used created the *cueSi36* transgene, hereafter called *Pmec-7::malsu-1::scarlet* to overexpress MALSU-1 in the PLM neuron. Consistent with work on mammalian MALSU1, we found that this overexpressed MALSU-1::SCARLET is localized to mitochondria (Fig. 6A-C).

We found that overexpression of MALSU-1 causes PLM axon termination defects that are significantly greater than those observed in controls (Fig. 6D). Overexpression of MALSU-1 also caused the axon beading phenotype (Fig. 6E). Finally, we found that overexpression of MALSU-1 decreases the average number of mitochondria in the PLM axon (Fig. 6F). These observations suggest that overexpression of MALSU-1 can cause axonal defects that are similar to those caused by loss of RBM-26 function.

Loss of MALSU-1 function suppresses the mitochondrial and axon degeneration phenotypes that are caused by loss of RBM-26 function.

Since overexpression of MALSU-1 causes phenotypes similar to loss of RBM-26, we hypothesized that RBM-26 prevents axon degeneration and targeting defects by negatively regulating MALSU-1 expression. This hypothesis predicts that the axonal defects caused by loss of RBM-26 function are dependent on MALSU-1 function. To test this prediction, we asked if loss of *malsu-1* function could suppress the axonal phenotypes caused by loss of *rbm-26* function (Fig. 7). For these experiments, we used the *malsu-1(syb6330)* allele, a near complete deletion of the *malsu-1* coding sequence. We found that the single *malsu-1(syb6330)* mutation did not cause the axon beading phenotype (Fig. 7A) or a reduction in the number of mitochondria (Fig. 7B). However, the *malsu-1(syb6330)* did cause significantly more PLM axon termination defects relative to wildtype (Fig. 7C).

If the *rbm-26* loss of function phenotypes are dependent on *malsu-1*, we would expect that *malsu-1; rbm-26* double mutants would have less axonal phenotypes relative to *rbm-26* single mutants. Since the *malsu-1* and *rbm-26* genes are tightly linked, we used CRISPR to introduce the P80L mutation into a strain containing the *malsu-1(syb6330)* mutation, thereby creating the *rbm-26(cue40 [P80L]);malsu-1(syb6330)* double mutant. We found that *rbm-26(cue40 [P80L]);malsu-1(syb6330)* double mutants have significantly lower penetrance of axon beading relative to *rbm-26(P80L)* single mutants (Fig. 7A). Likewise, *rbm-26(cue40 [P80L]);malsu-1(syb6330)* double mutants also have significantly more mitochondria relative to *rbm-26(P80L)* single mutants (Fig. 7B). For the case of axon termination, we would not expect to see a suppression of the *rbm-26(P80L)* phenotype by *malsu-1(syb6330)*, because *malsu-1(syb6330)* single mutants already have axon termination defects that are equal in penetrance to *rbm-26(P80L)* mutants. However, we did find that *rbm-26(cue40 [P80L]);malsu-1(syb6330)* double mutants had a penetrance of axon termination defects that was equal to *malsu-1(syb6330)* single mutants (Fig. 7C), consistent with the function of *malsu-1* and *rbm-26* in a genetic pathway. To validate these findings, we also repeated these experiments with an independent allele of *malsu-1*, *malsu-1(tm12122)* and found similar results (Fig. 7A-C). Taken together, these observations indicate that the axonal phenotypes of *rbm-26(P80L)* mutants are dependent on MALSU-1 function. Moreover, these observations are consistent with the hypothesis that RBM-26 prevents axon degeneration and targeting defects by negatively regulating MALSU-1 activity.

Loss of RBM-26 function reduces levels of mitoribosome marker.

MALSU1 is a negative regulator of mitoribosome assembly, prompting us to hypothesize that the excess levels of MALSU-1 expression in *rbm-26* mutants disrupt formation of mitoribosomes. To test this hypothesis, we used a strategy called mitoRiboTag, which has previously been used in mice [30]. To adopt this technique for *C. elegans*, we used CRISPR to add a 3XFLAG tag to the C-terminus of the MRPL-58 protein, a component of mitoribosomes, thereby creating the *mrpl-58(cue38)* allele, which expresses the MRPL-58::3XFLAG protein. Consistent with our hypothesis, we found that loss of *rbm-26* function causes a robust decrease in the levels of MRPL-58::3XFLAG protein relative to wild type (Fig. 8). This observation suggests that loss of *rbm-26* causes a disruption of mitoribosomes.

Discussion

Here, we report that RBM-26 functions in the nuclei of neurons to regulate expression of the MALSU-1 mitoribosome assembly factor. RBM-26 binds to the *malsu-1* mRNA and sharply reduces its expression. Disruptions in this process cause a sharp reduction in mitoribosome levels, leading to mitochondrial dysfunction along with defects in axon

targeting and degeneration of developing axons. These observations provide an example of how post-transcriptional regulation of an mRNA in the nucleus can protect mitochondria in the axon to prevent axon degeneration and targeting defects. Moreover, our results also suggest that disruption of this process can give rise to neurodevelopmental disorders.

Emerging evidence for the role of the nuclear RNA exosome in the regulation of neurodevelopment and neurodegeneration.

The negative regulation of *malsu-1* mRNA by RBM-26 may occur through the process of mRNA decay in the nucleus. This idea is supported by our finding that RBM-26 is localized to the nucleus and negatively regulates *malsu-1* mRNA. Moreover, prior work in human cells has indicated that RBM26/27 functions with the PAXT complex, an adaptor that delivers polyadenylated RNA to the nuclear RNA exosome for degradation [17]. A similar complex exists in *S. pombe*, where the Rmn1 protein is an ortholog of RBM-26 and functions with the MTREC complex, which is orthologous to the PAXT complex [18]. Thus, RBM-26 is part of a highly conserved complex that collaborates with the nuclear RNA exosome to negatively regulate polyadenylated RNA.

Although most work on the nuclear RNA exosome complex has focused on non-coding nuclear RNAs, emerging evidence suggests that this complex is also important for the regulation of some mRNAs. For example, in *S. pombe*, the MTREC complex is orthologous to the PAXT complex and is critical for the suppression of meiosis. In this process, the MTREC complex binds to the mRNAs of meiotic genes and delivers them to the nuclear RNA exosome for degradation [31]. In cultured human cells, the *PABPN1* mRNA is degraded by the nuclear RNA exosome, thereby negatively regulating both the *PABPN1 mRNA* and the PABPN protein [32]. In addition, knockdown of RBM26/27 or other members of the PAXT complex in HeLa cells can cause upregulation of more than 1000 mRNAs, suggesting that the PAXT complex is able to regulate mRNAs [17]. Consistent with this finding, a group of 360 full length protein-coding mRNAs were identified that are regulated by the nuclear mRNA exosome in HeLa cells [33]. Together, these observations indicate that the PAXT complex can function with the nuclear RNA exosome to regulate some protein-coding mRNA transcripts.

The axon degeneration and neurodevelopmental phenotypes caused by *rbm-26* mutations are reminiscent of phenotypes caused by mutations in subunits of the human RNA exosome complex. For example, pedigree analysis has indicated that mutations in the *EXOSC3*, EXOSC8 and EXOSC9 can cause syndromes that include defects in brain development such as hypoplasia of the cerebellum and the corpus callosum [12-14, 34, 35]. In addition, these syndromes also involve progressive neurodegeneration of spinal neurons that begins in infancy and resembles spinal motor atrophy (SMA). Consistent with these observations, knockdown of EXOSC3, EXOSC8, and EXOSC9 in zebrafish causes brain malformation and axon pathfinding defects [12, 34, 36].

Moreover, mutations in EXOSC3 and EXOSC9 also cause intellectual disability in humans [14, 35] and mutations in EXOSC8 causes behavioral defects in zebrafish [34]. Together, these observations suggest an important role in for the RNA exosome complex in protecting against neurodegeneration and preventing neurodevelopmental defects.

Potential role for MALSU-1 overexpression in the disruption of mitoribosome biogenesis.

The biogenesis of mitoribosomes is a complex process that involves the assembly of 80 proteins and 2 rRNAs into a large subunit (mtLSU) and a small subunit (mtSSU). This process is facilitated by a large number of mitoribosomal assembly factors including RNA processing enzymes, GTPases, RNA helicases, and kinases. MALSU-1 is a mitoribosomal assembly factor that functions as part of the MALSU1:LOR8F8:mtACP anti-association module [37-39]. This module binds to the mtLSU and blocks premature association of mtLSU with mtSSU. Once assembly of mtLSU is complete, MALSU1:LOR8F8:mtACP is released, thereby allowing association of mtLSU with mtSSU. Consistent with these observations, knockdown of MALSU1 in cultured human cells causes mitochondrial dysfunction by disrupting the formation of mitoribosomes [29].

Our results suggest that the excessive expression of MALSU-1 can also disrupt mitochondria. We propose that this disruption of mitochondria occurs because excess MALSU-1 can disrupt mitoribosome assembly. This idea is supported by our finding that loss of RBM-26 function disrupts expression of MRPL-58::3XFLAG, a marker for mitoribosomes. This idea is also consistent with our finding that loss of *rbm-26* function causes a very high level of MALSU-1 protein, a negative regulator of mitoribosome assembly. Moreover, the axon and mitochondrial defects caused by loss of RBM-26 function are dependent on MALSU-1 expression. Under normal conditions, MALSU1 binds to mtLSU and prevents it from prematurely assembling with mtSSU [37-39]. After completion of mtLSU assembly, MALSU1 is released, thereby allowing for binding of mtLSU and mtSSU. We hypothesize that the high level of MALSU-1 expression in *rbm-26* mutants may prevent the dissociation of MALSU-1 from the mtLSU, thereby interfering with the association between mtLSU and mtSSU.

Our results suggest that the overexpression of MALSU-1 is more detrimental than the loss of MALSU-1 function. We found that loss of MALSU-1 causes axon termination defects that are comparable to loss of *rbm-26* function. However, we found that loss of MALSU-1 function did not cause axon beading nor did it cause a reduction in the number of mitochondria. These observations could be explained by the fact that MALSU1 might function with partial redundancy with two other assembly factors, LOR8F8 and mtACP. In this scenario, LOR8F8 and mtACT would still have partial ability to block the premature assembly of the two mitoribosome subunits. On the other

hand, LOR8F8 and mtACP would not be expected to mitigate the defects caused by excessive expression of MALSU-1. Therefore, it is possible that disruption in the post transcriptional regulation of mitoribosomal assembly factors may represent a key vulnerability for mitoribosome-associated disease.

Materials and Methods

Strains: The alleles used in this study are listed in supplemental table 2. The *rbm-26(gk910)* mutation is lethal and was maintained over the hT2 balancer marked with *bli-4* and *(qIs48)*. Worms used for phenotype analysis were maintained at 20°C on nematode growth medium (NGM) agar plates seeded with OP50 using standard procedures. Worms used for RNA Immunoprecipitation experiments and Western Blotting were cultured on 8P plates seeded with *E. coli* NA22 strain as food source.

Genome editing: Genome editing for *malsu-1(syb6330)* and *rbm-26(*syb2552 [*rbm-26::scarlet::AID]*) were performed by Suny Biotech. All other genome editing was performed in our laboratory using a previously described protocol [40]. Guide RNAs and homology directed repair (HDR) templates are listed in supplemental table 3. CRISPR edits were confirmed via PCR and sequencing.

Transgenes: The *cueSi36 transgene* encodes *Pmec7::malsu-1::scarlet::tbb-2 3'UTR* and the *cueSi35* transgene encodes *Pmec-7:mitoTimer::tbb-2 3'UTR*. A single copy of these transgenes was inserted into the *jsTi1493* landing pad on chromosome IV using the Flp recombinase mediated cassette exchange (RMCE) protocol [41]. The *muIs32* transgene is an integrated multicopy array that encodes *Pmec7::GFP* and was used to visualize the PLM axon. The *jsIs1073* transgene was obtained from Michael Nonet and *encodes Pmec-7::mts:tagRFP* and expresses mitochondria-targeted TagRFP (mitoTagRFP). The *jsIs609* transgene was also obtained from Michael Nonet and encodes *Pmec-7::mts::GFP* and expresses a mitochondria-targeted GFP (mitoGFP) in the PLM neuron

Analysis of phenotypes: To quantify phenotypes, worms were mounted on a 5% agarose pad, anesthetized with levamisole, and observed with a 40x objective on a Zeiss Axio Imager M2 microscope. PLM axons were visualized using the *muIs32 (Pmec-7::GFP)* transgene. A PLM axon was considered overextended if the axon tip terminated anteriorly to the ALM cell body. Beading refers to focal enlargement or bubble-like lesions which were at least twice the diameter of the axon in size.

Imaging: Larval stage images displayed in all figures were obtained by mounting on 5% agarose pad, anesthetizing with levamisole, and imaging with a 60x water objective on a Nikon ECLIPSE Ti microscope equipped with the X-Light V2 L-FOV spinning disk system. NIS-Elements software was used for image acquisition. Image analysis was done with ImageJ or NIS-elements. Identical imaging settings and look-up-tables were

used for control and experimental groups. Imaging for mitochondrial counts was done with a 40X oil objective on a Zeiss Axio Imager M2.

Analysis of mitoTimer: All images were captured with identical settings on a spinning disk confocal system (see above). 8-bit images were opened in ImageJ in both red and green channels, the PLM cell body was traced in one channel with the free hand selection tool, and the tracing was restored in the other channel. Raw Integrated Density (RawIntDen) and the area of the region of interest (ROI) was determined in ImageJ. Similarly, RawIntDen and area of a defined background region was obtained. RawIntDen was divided by the area of ROI to obtain total pixel/area. Corrected total pixel/area was obtained by subtracting the background pixel/area from the ROI for both red and green channels.

Auxin mediated protein degradation: Tissue-specific degradation of RBM-26::Scarlet::AID was carried out using the auxin-induced degron (AID) system as previously described [42]. Briefly, Naphthaleneacetic acid (K-NAA) (Phytotechnology Laboratories) was dissolved in double distilled water to obtain 250 mM K-NAA solution and filter-sterilized by passing through 25 mm sterile syringe filter (Pall Corporation). Aliquots from sterile 250 mM K-NAA stock was added to autoclaved and slightly cooled (60°C) NGM to obtain a concentration of 4 mM K-NAA, and poured into plates. The next day, 4mM K-NAA plates were seeded with 250 ul *E. coli* OP50 strain. These plates were used within two weeks. L4 stage *C. elegans* of different genotypes were placed on 4 mM K-NAA plates, allowed to grow and lay eggs, L3 stage progenies of the parents initially placed on 4 mM K-NAA plates were analyzed for PLM overextensions and PLM beading phenotypes. PLMs were visualized with *Pmec-7::GFP* transgene*. rbm-26::Scarlet::AID* without any TIR1 cofactor of AID made up the control group.

UV-crosslinking RNA Immunoprecipitation and RNA-Seq: Worms expressing *wbmIs67* transgene *(eft-3p::3X FLAG::Scarlet::unc-54 3'UTR)* and *wbmIs72* transgene *(pei-1p::3X FLAG::GFP::unc-54 3'UTR)* were used as control group. Control and *rbm-26::3X FLAG* worms were grown on NGM plates seeded with *E. coli* OP50 strain until they became gravid, then they were washed in M9 (22mM KH2PO4; 22mM Na2HPO4; 85mM NaCl; 1mM MgSO4) and grown for 2 days on 8P plates seeded with *E. coli* strain NA22. 25,000 mixed stages *C. elegans* were washed three times in M9 and placed in an unseeded NGM plate (10 cm) for UV-crosslinking. Plate covers and liquid were removed, and the NGM plates were placed in Spectrolinker X-1000 (Spectronics Corporation) and irradiated with 254 nm UV at energy setting 3000. Worms were then checked under the microscope to ensure that they were immobilized, following which they were washed in M9, and 100,000 worms were collected in 1 ml of RIPA buffer (50 mM Tris HCl pH 7.4, 150 mM NaCl, 1% Nonidet NP-40, 0.1% SDS, 0.5% Sodium deoxycholate, Roche cOmplete EDTA-free Protease Inhibitor Cocktail, 25U/ml RNase inhibitor) and homogenized/lysed in BeadBug™3 Microtube homogenizer (40 second homogenization with 1 min rest on ice) at 4°C with 3.2 mm diameter chrome steel beads

(8 beads per tube). Lysates were placed in fresh tubes, centrifuged at 16,000 xG for 15 mins at 4°C. The supernatant was saved as lysate and quantified using Pierce BCA Protein Assay kit. 100 ul of Pierce Anti-DYKDDDDK (anti-FLAG) magnetic agarose resin was washed three times in RIPA buffer and added to 1 ml of protein lysate (2 mg/ml), incubated overnight at 4°C, and anti-flag agarose bound lysate was separated with the help of a magnet while the supernatant was discarded. The agarose resin was washed once with high salt buffer (50 mM Tris HCl pH 7.4, 1M NaCl, 1 mM EDTA, 1% Nonidet NP-40, 0.1% SDS, 0.5% Sodium deoxycholate, Roche cOmplete EDTA-free Protease Inhibitor Cocktail and RNase Inhibitor) and three times with low salt buffer (20 mM Tris HCl pH 7.4, 10mM $MgCl_2$, 0.2% Tween-20, Roche Protease Inhibitor and RNase Inhibitor). To elute RNA, the agarose resin was dissolved in Proteinase K buffer (50 mM Tris-HCl, pH 7.4, 150 mM NaCl, 1 mM MgCl2, 0.05% NP-40, 1% SDS) and incubated with 1.2 mg/ml Proteinase K at 55°C for 30 mins with gentle agitation. RNA was extracted with phenol:chloroform and precipitated with 0.25M Ammonium Acetate, 0.12M Lithium Chloride and 85% Ethanol. The pellets were washed with 75% ethanol, dissolved in DEPC-treated water and sent to Azenta US, Inc. for library preparation and RNA sequencing.

Raw data obtained from Azenta US, Inc. was analyzed to identify RNA interactors of RBM-26. For RNA-Sequencing pre-processing, adapters were trimmed using Cutadapt [43], and contaminating rRNA reads were removed using bowtie2 [44, 45]. Reads were mapped to the Caenorhabditis elegans transcriptome (Caenorhabditis_elegans.WBcel235) using STAR [46] and differential gene analysis was performed using the DESeq2 package [47] in R Studio. Mapped reads were sorted and indexed using samtools [48].

Absolute quantification of *malsu-1* mRNA:300 N2 wild-type L4 worms and 300 *rbm-26(cue23)* L4 worms were collected in Trizol. Following 5 rounds of freeze thaw on dry-ice with 1 min of vortexing during thawing, RNA was extracted as per the manufacturer's protocol.

We purchased the following synthetic RNA from Azenta US, Inc:
GCACGAAGGAGCACAAAACGAAGCAAUGGAUGGUAUGUCAGUGAGGUGGAAAGA
GUUCAGGUGCACG

The synthetic RNA was diluted in nuclease free water and the following concentrations were confirmed with Qubit RNA Broad Range Assay Kit (Thermo Fisher Scientific): 10 ng/ul, 1 ng/ul, 0.1 ng/ul, 0.01 ng/ul, 0.001 ng/ul, and 0.0001 ng/ul. The diluted RNA (standards) and 1 ug of total RNA extracted from wildtype and *rbm-26(cue23)* L4 worms were reverse transcribed with 2μm reverse primer (CGTGCACCTGAACTCTTTCC) and Superscript^{TM} First-Strand Synthesis System (Thermo Fisher Scientific) following the manufacturer's protocol. 1μl cDNA was used with 10μl 2x SsoAdvanced Universal SYBR Green Supermix (Biorad) and 5 pmol of the forward *malsu-1* primer

(TGCACGAAGGAGCACAAAAC) and the reverse *malsu-1* primer (CGTGCACCTGAACTCTTTCC). Fluorescence emitted during each cycle was monitored using the CFX96 Touch Real-Timer PCR Detection System (Biorad). Dissociation curve confirmed the presence of a single amplicon. Cycle-to-Threshold (Ct) value of the RNA standards were used to plot a standard curve (R^2 = 0.995), which was then used to deduce *malsu-1* mRNA quantity. Data presented here comes from three biological replicates.

Western Blotting: Worms were grown on NGM plates seeded with *E. coli OP50* until gravid, washed in M9, and plated onto 8P plates seeded with *E. coli NA22*. 50,000 worms were collected in M9, washed three times and M9 was replaced with RIPA buffer (50,000 worms/1 ml RIPA buffer). Worms were lysed in Bead Bug™3 Microtube homogenizer at 4°C with 3.2 mm chrome steel beads (8 beads/ml RIPA buffer). Following centrifugation at 16000 xg for 15 mins at 4°C, supernatant was saved (snap-frozen) as total protein lysate and pellet was dissolved in 0.8M Urea and snap-frozen. Total protein lysate and pellet fraction were quantified through BCA assay. 20 – 25 μg of total protein lysate was run on either 7.5% or 12% SDS-PAGE, transferred to nitrocellulose membrane (0.2 μm pore), blocked in 5% non-fat milk in TBST (20 mM Tris, 150 mM NaCl, 0.1 % Tween-20), probed with primary antibody, washed three times in TBST, probed with secondary antibody, developed with Western Blue Stabilized Substrate for Alkaline Phosphatase (Promega) or with Super Signal West PICO Plus (Thermo Fisher Scientific) and imaged with iBright 1500 (Thermo Fisher Scientific). Antibodies used in this study are listed in supplemental table 4. Immunoblot in figure 5 was stripped, washed three times in TBST and re-probed with loading control primary antibody and corresponding secondary antibody.

Acknowledgements

We thank Michael Nonet and the Caenorhabditis Genetics Center (funded by NIH P40 OD010440) for strains. We also thank Claire de la Cova and Mark McBride for sharing equipment, Claire de la Cova for assistance with imaging experiments and Scott Aoki for help with the UV-RIPseq experiments. This work was funded by the National Institute of Mental Health grant R01MH119157 (to CCQ), the National Institute of Neurological Disorders and Stroke grant R03NS101524 (to CCQ), Discovery and Innovation Grant (101X432) from the University of Wisconsin - Milwaukee (to TAC) and National Institutes of Health grant 1R35GM142527 (to ASYL). This article does not represent the official views of the National Institutes of Health and the authors bear sole responsibility for its content.

Figure Legends

Figure 1: Expression of RBM-26 is disrupted by P80L and L13V missense mutations. (A) Putative protein domains in human RBM27, and *C. elegans* RBM-26 proteins predicted by NCBI's CD-Search. CCCH-type Zn Finger domains (Green Rectangles) and RNA Recognition Motifs (Gold Pentagons) were predicted with high confidence by NCBI's CD-Search and SMART database. PWI superfamily (Blue Hexagon) was predicted by NCBI's CD-Search with high confidence. Red arrows indicate de novo missense variants identified in patients with autism or intellectual disability. (B) Clustal Omega alignment of the N-terminus of the human RBM27 and *C. elegans* RBM-26 proteins. Two de novo RBM27 variants, L13V and P79L (red arrows), were found in regions conserved in *C. elegans* RBM-26. (C) Representative western blot showing expression of RBM-26::3XFLAG, RBM-26 P80L::3XFLAG and RBM-26 L13V::3XFLAG proteins. The sequence encoding 3XFLAG was inserted just upstream of the stop codon in the *rbm-26* gene to create the *rbm-26(cue25)* allele, which expresses the RBM-26::3XFLAG protein. A second round of editing was done on this allele to create the *rbm-26(cue22)* mutation that expresses the RBM-26 P80L::3XFLAG protein and the *rbm-26(cue34)* mutation that expresses the RBM-26 L13V::3XFLAG protein. 20 μg of total protein lysate was loaded per well and specific proteins were detected with an anti-FLAG primary antibody, goat anti-rabbit secondary antibody and NBT/BCIP colorimetric detection. Equal loading was achieved by protein assay and confirmed by Ponceau S staining.

Figure 2: Mutations in *rbm-26* cause axon degeneration and defects in axon targeting. (A) Example of normal PLM axon termination in a wild-type L3 stage worm. (B) Diagram of the touch receptor neurons. The inset shows where the PLM axon terminates in relation to ALM cell body. (C) Example of PLM axon termination defect (arrow) in an *rbm-26(null)* mutant; axon beading can also be seen (asterisk). (D) Quantification of axon termination defects in *rbm-26* mutants. (E) Example of axon beading phenotype (asterisks) in an *rbm-26(null)* mutant. (F) Quantification of beading phenotype in *rbm-26* mutants In panels D and F, the number of PLMs scored (n) for wt is 182, n for *rbm-26(null)* is 203, n for *rbm-26(P80L)* is 193 and n for *rbm-26(L13V)* is 204. Asterisks indicate statistically significant difference relative to wild type, Z-test for proportions (*** $p<0.0001$), and error bars represent the standard error of the proportion. Scale bars are 10 μm.

Figure 3: RBM-26 is expressed in multiple tissues and functions within neurons to protect against neurodegeneration and prevent defects in axon targeting. (A-D) RBM-26 is expressed in the nuclei of neurons and hypodermal cells. Neurons are identified by the pan-neuronal expression of GFP by the *evIs111* transgene (panels A and D). Hypodermal nuclei are identified by tissue-specific expression of blue

fluorescent protein tagged with a nuclear localization signal and an auxin-induced degron (AID) (panels C and D). “N” in panels A, B, and D indicate neuron and “Hn” in panels B, C, and D indicate hypodermal nuclei. Scale bar is 10 μm. (E-F) Neuron specific degradation of RBM-26::SCARLET::AID causes PLM axon overextension and PLM axon beading. However, degradation in hypodermis, muscle and intestine do not cause these phenotypes. Tissue specific degradation of RBM-26::SCARLET::AID was achieved due to cell-type specific TIR-1 driver lines (see methods for details). Control strain is *rbm-26::Scarlet::AID*. Asterisks indicate statistically significant difference, Z-test for proportions (* $p<0.05$), and error bars represent the standard error of the proportion.

Figure 4: Loss of RBM-26 causes mitochondria dysfunction in axons. (A-E) RBM-26 loss of function reduces the number of mitochondria in the PLM axon. (A-B) Example of mitochondria (arrowheads) in an L3 wild-type PLM axon. (C-D) Example of mitochondria in an L3 *rbm-26(null)* mutant PLM axon. (E) Quantification of the number of mitochondria in L3 *rbm-26* mutant PLM axons (n=35 for each genotype). The PLM axon was visualized with the *muIs32* transgene, which encodes *Pmec-7::gfp.* Mitochondria were visualized with the *jsIs1073* transgene, which *encodes Pmec-7::mito:RFP* and expresses mitochondria-targeted TagRFP (mitoTagRFP). Scale bars are 10 μm. (F-I) RBM-26 loss of function causes excess oxidative activity in mitochondria. To detect oxidative activity in mitochondria, we used mitoTimer, which is a green fluorescent protein when newly synthesized but shifts to red fluorescence when oxidized. (F-F’’) Example of mitoTimer expression in an L4 wild-type PLM cell body. (G-G’’) Example of mitoTimer expression in an L4 *rbm-26(P80L)* mutant PLM cell body. Scare bars are 2 μm. (H) Quantification of the ratio of red to green mitoTimer expression in wt and *rbm-26(P80L)* L4 PLM cell body (n = 25 each). (I) Quantification of the ratio of red to green mitoTimer expression in wt and *rbm-26(null)* L2 PLM cell bodies (n = 20 each). Asterisks in panels C, H and I indicate statistically significant difference (two-tailed student’s t-test) relative to wild-type control (*$p<0.05$, **$p<0.01$, ***$p<0.0001$).

Figure 5: RBM-26 binds to the *malsu-1* mRNA and negatively regulates its expression. (A) Six classes of RNA interactors of RBM-26 as identified by UV-RIPseq (see methods for details). Twelve mRNAs were identified with human orthologs, including *malsu-1* (black arrow). Data generated from three biological replicates. (B) Loss of RBM-26 function increases expression of the *malsu-1* mRNA. Absolute levels of *malsu-1* mRNA quantified using real-time RT-PCR (see methods for details). Graph represents average of three biological replicates. Error bars are standard deviation. Asterisks indicate statistically significant difference relative to wild type, two-tailed student’s t test (***$p<0.0001$). (C) Loss of RBM-26 function causes an increase in MALSU-1 protein expression. 20 μg of total protein lysate from a mixed stage population was loaded per well and specific proteins were detected with an anti-FLAG or anti-TUBULIN antibody and enhanced chemiluminescence. Equal loading was

achieved by protein assay and confirmed by blotting with an anti-TUBULIN antibody. Western blot is representative of two biological replicates.

Figure 6: Overexpression of MALSU-1 reduces mitochondria in the PLM axon and causes axon degeneration and defects in axon targeting. (A-C) Overexpressed MALSU-1::SCARLET protein colocalizes with mitochondria. (A) Mitochondria visualized with the *jsIs609* transgene, which expresses a mitochondria-targeted GFP (mitoGFP) in the PLM neuron. (B) MALSU-1::SCARLET expressed by the *cueSi36* transgene. (C) Merged image showing colocalization of MALSU-1::SCARLET with mitoGFP. (D-F) Overexpression of MALSU-1::SCARLET causes defects similar to those caused by loss of RBM-26 function. (D) Axon termination defects caused by MALSU-1::SCARLET overexpression. (E) PLM axon beading phenotype caused by MALSU-1::SCARLET overexpression. (F) Decrease in mitochondria in the PLM axon caused by MALSU-1::SCARLET overexpression. Asterisks indicate statistically significant difference relative to wild type, Z-test for proportions (**$p<0.01$, ***$p<0.0001$). For panels D and E, error bars represent the standard error of the proportion. For panel F, error bars represent the standard error of the mean.

Figure 7: Loss of MALSU-1 function suppresses the mitochondrial and axon degeneration phenotypes that are caused by loss of RBM-26 function. (A) Loss of *malsu-1* function suppresses the PLM axon beading phenotype caused by the loss of *rbm-26* function. (B) Loss of *malsu-1* function suppresses the reduction of mitochondria caused by the loss of *rbm-26* function. (C) Loss of *malsu-1* function causes PLM axon overextension defects but fails to enhance PLM axon overextension defects caused by the loss of *rbm-26* function. The *rbm-26(cue40 [P80L]); malsu-1(syb6330)* double mutant was created by introducing the P80L mutation into the *malsu-1(syb6330)* mutant chromosome. The *rbm-26(cue41 [P80L]; malsu-1(tm12122)* double mutant was created by introducing the P80L mutation into the *malsu-1(tm12122)* mutant chromosome. Asterisks indicate statistically significant difference, Z-test for proportions (*$p<0.05$, **$p<0.01$, *** $p<0.0001$). For panels A and C, error bars represent the standard error of the proportion. For panel B, error bars represent the standard error of the mean.

Figure 8: Loss of RBM-26 function reduces expression of a mitoribosome marker. Mitoribosome expression was assayed with the MitoRibo-Tag system, which consists of the MRPL-58 mitoribosomal protein tagged at its C-terminus with 3XFLAG (MRPL-58::3XFLAG). This MRPL-58::3XFLAG protein was expressed by the *mrpl-58(cue38)* allele, which was created by CRISPR. CRISPR was also used to introduce the RBM-26 P80L variation into a strain containing the *mrpl-58(cue38)* allele, thereby creating the *mrpl-58(cue38)*; *rbm-26(cue39)* double mutant. The wt lane consists of *mrpl-58(cue38)* lysate. The *rbm-26(P80L)* lane consists of *mrpl-58(cue38)*; *rbm-26(cue39)* lysate. 25μg

of total protein lysate was loaded per lane and specific proteins were detected with an anti-FLAG or anti-TUBULIN antibodies and enhanced chemiluminescence. Equal loading was achieved by protein assay and confirmed by blotting with an anti-TUBULIN antibody. Results shown are representative of two biological replicates.

Literature Cited

1. Chalkia, D., et al., *Association Between Mitochondrial DNA Haplogroup Variation and Autism Spectrum Disorders.* JAMA Psychiatry, 2017. **74**(11): p. 1161-1168.
2. Chang, X., et al., *Mitochondrial DNA haplogroups and risk of attention deficit and hyperactivity disorder in European Americans.* Transl Psychiatry, 2020. **10**(1): p. 370.
3. Valiente-Palleja, A., et al., *Genetic and clinical evidence of mitochondrial dysfunction in autism spectrum disorder and intellectual disability.* Hum Mol Genet, 2018. **27**(5): p. 891-900.
4. Wang, Y., et al., *Association of mitochondrial DNA content, heteroplasmies and inter-generational transmission with autism.* Nat Commun, 2022. **13**(1): p. 3790.
5. Wang, Y., M. Picard, and Z. Gu, *Genetic Evidence for Elevated Pathogenicity of Mitochondrial DNA Heteroplasmy in Autism Spectrum Disorder.* PLoS Genet, 2016. **12**(10): p. e1006391.
6. Yardeni, T., et al., *An mtDNA mutant mouse demonstrates that mitochondrial deficiency can result in autism endophenotypes.* Proc Natl Acad Sci U S A, 2021. **118**(6).
7. Liu, X., et al., *Oxidative Stress in Autism Spectrum Disorder-Current Progress of Mechanisms and Biomarkers.* Front Psychiatry, 2022. **13**: p. 813304.
8. Cousin, M.A., et al., *Pathogenic SPTBN1 variants cause an autosomal dominant neurodevelopmental syndrome.* Nat Genet, 2021. **53**(7): p. 1006-1021.
9. Leite, S.C., et al., *The Actin-Binding Protein alpha-Adducin Is Required for Maintaining Axon Diameter.* Cell Rep, 2016. **15**(3): p. 490-498.
10. Lorenzo, D.N., et al., *betaII-spectrin promotes mouse brain connectivity through stabilizing axonal plasma membranes and enabling axonal organelle transport.* Proc Natl Acad Sci U S A, 2019. **116**(31): p. 15686-15695.
11. Qi, C., et al., *Variants in ADD1 cause intellectual disability, corpus callosum dysgenesis, and ventriculomegaly in humans.* Genet Med, 2022. **24**(2): p. 319-331.
12. Burns, D.T., et al., *Variants in EXOSC9 Disrupt the RNA Exosome and Result in Cerebellar Atrophy with Spinal Motor Neuronopathy.* Am J Hum Genet, 2018. **102**(5): p. 858-873.
13. Wan, J., et al., *Mutations in the RNA exosome component gene EXOSC3 cause pontocerebellar hypoplasia and spinal motor neuron degeneration.* Nat Genet, 2012. **44**(6): p. 704-8.
14. Zanni, G., et al., *Exome sequencing in a family with intellectual disability, early onset spasticity, and cerebellar atrophy detects a novel mutation in EXOSC3.* Neurogenetics, 2013. **14**(3-4): p. 247-50.
15. Shirakaki, S., R.R. Roshmi, and T. Yokota, *Genetic Approaches for the Treatment of Giant Axonal Neuropathy.* J Pers Med, 2022. **13**(1).

16. Abrahams, B.S., et al., *SFARI Gene 2.0: a community-driven knowledgebase for the autism spectrum disorders (ASDs).* Mol Autism, 2013. **4**(1): p. 36.
17. Silla, T., et al., *The human ZC3H3 and RBM26/27 proteins are critical for PAXT-mediated nuclear RNA decay.* Nucleic Acids Res, 2020. **48**(5): p. 2518-2530.
18. Zhou, Y., et al., *The fission yeast MTREC complex targets CUTs and unspliced pre-mRNAs to the nuclear exosome.* Nat Commun, 2015. **6**: p. 7050.
19. Ariyapala, I.S., et al., *The RNA-binding protein Swm is critical for Drosophila melanogaster intestinal progenitor cell maintenance.* Genetics, 2022. **222**(2).
20. Pan, C.L., et al., *Genetic analysis of age-dependent defects of the Caenorhabditis elegans touch receptor neurons.* Proc Natl Acad Sci U S A, 2011. **108**(22): p. 9274-9.
21. Tank, E.M., K.E. Rodgers, and C. Kenyon, *Spontaneous age-related neurite branching in Caenorhabditis elegans.* J Neurosci, 2011. **31**(25): p. 9279-88.
22. Toth, M.L., et al., *Neurite sprouting and synapse deterioration in the aging Caenorhabditis elegans nervous system.* J Neurosci, 2012. **32**(26): p. 8778-90.
23. Burke, R.E. and K. O'Malley, *Axon degeneration in Parkinson's disease.* Exp Neurol, 2013. **246**: p. 72-83.
24. Yong, Y., et al., *Axonal spheroids in neurodegeneration.* Mol Cell Neurosci, 2021. **117**: p. 103679.
25. Yuan, P., et al., *PLD3 affects axonal spheroids and network defects in Alzheimer's disease.* Nature, 2022. **612**(7939): p. 328-337.
26. Murphy, M.P., *How mitochondria produce reactive oxygen species.* Biochem J, 2009. **417**(1): p. 1-13.
27. Schon, E.A. and S. Przedborski, *Mitochondria: the next (neurode)generation.* Neuron, 2011. **70**(6): p. 1033-53.
28. Laker, R.C., et al., *A novel MitoTimer reporter gene for mitochondrial content, structure, stress, and damage in vivo.* J Biol Chem, 2014. **289**(17): p. 12005-12015.
29. Rorbach, J., P.A. Gammage, and M. Minczuk, *C7orf30 is necessary for biogenesis of the large subunit of the mitochondrial ribosome.* Nucleic Acids Res, 2012. **40**(9): p. 4097-109.
30. Busch, J.D., et al., *MitoRibo-Tag Mice Provide a Tool for In Vivo Studies of Mitoribosome Composition.* Cell Rep, 2019. **29**(6): p. 1728-1738 e9.
31. Harigaya, Y., et al., *Selective elimination of messenger RNA prevents an incidence of untimely meiosis.* Nature, 2006. **442**(7098): p. 45-50.
32. Bergeron, D., et al., *Regulated Intron Retention and Nuclear Pre-mRNA Decay Contribute to PABPN1 Autoregulation.* Mol Cell Biol, 2015. **35**(14): p. 2503-17.
33. Wu, M., et al., *The RNA exosome shapes the expression of key protein-coding genes.* Nucleic Acids Res, 2020. **48**(15): p. 8509-8528.
34. Boczonadi, V., et al., *EXOSC8 mutations alter mRNA metabolism and cause hypomyelination with spinal muscular atrophy and cerebellar hypoplasia.* Nat Commun, 2014. **5**: p. 4287.
35. Di Donato, N., et al., *Mutations in EXOSC2 are associated with a novel syndrome characterised by retinitis pigmentosa, progressive hearing loss, premature ageing, short stature, mild intellectual disability and distinctive gestalt.* J Med Genet, 2016. **53**(6): p. 419-25.

36. Giunta, M., et al., *Altered RNA metabolism due to a homozygous RBM7 mutation in a patient with spinal motor neuropathy.* Hum Mol Genet, 2016. **25**(14): p. 2985-2996.
37. Brown, A., et al., *Structures of the human mitochondrial ribosome in native states of assembly.* Nat Struct Mol Biol, 2017. **24**(10): p. 866-869.
38. Cheng, J., O. Berninghausen, and R. Beckmann, *A distinct assembly pathway of the human 39S late pre-mitoribosome.* Nat Commun, 2021. **12**(1): p. 4544.
39. Rebelo-Guiomar, P., et al., *A late-stage assembly checkpoint of the human mitochondrial ribosome large subunit.* Nat Commun, 2022. **13**(1): p. 929.
40. Ghanta, K.S., T. Ishidate, and C.C. Mello, *Microinjection for precision genome editing in Caenorhabditis elegans.* STAR Protoc, 2021. **2**(3): p. 100748.
41. Nonet, M.L., *Efficient Transgenesis in Caenorhabditis elegans Using Flp Recombinase-Mediated Cassette Exchange.* Genetics, 2020. **215**(4): p. 903-921.
42. Martinez, M.A.Q. and D.Q. Matus, *Auxin-mediated Protein Degradation in Caenorhabditis elegans.* Bio Protoc, 2020. **10**(8).
43. Kechin, A., et al., *cutPrimers: A New Tool for Accurate Cutting of Primers from Reads of Targeted Next Generation Sequencing.* J Comput Biol, 2017. **24**(11): p. 1138-1143.
44. Langmead, B. and S.L. Salzberg, *Fast gapped-read alignment with Bowtie 2.* Nat Methods, 2012. **9**(4): p. 357-9.
45. Langmead, B., et al., *Scaling read aligners to hundreds of threads on general-purpose processors.* Bioinformatics, 2019. **35**(3): p. 421-432.
46. Dobin, A., et al., *STAR: ultrafast universal RNA-seq aligner.* Bioinformatics, 2013. **29**(1): p. 15-21.
47. Love, M.I., W. Huber, and S. Anders, *Moderated estimation of fold change and dispersion for RNA-seq data with DESeq2.* Genome Biol, 2014. **15**(12): p. 550.
48. Li, H., et al., *The Sequence Alignment/Map format and SAMtools.* Bioinformatics, 2009. **25**(16): p. 2078-9.

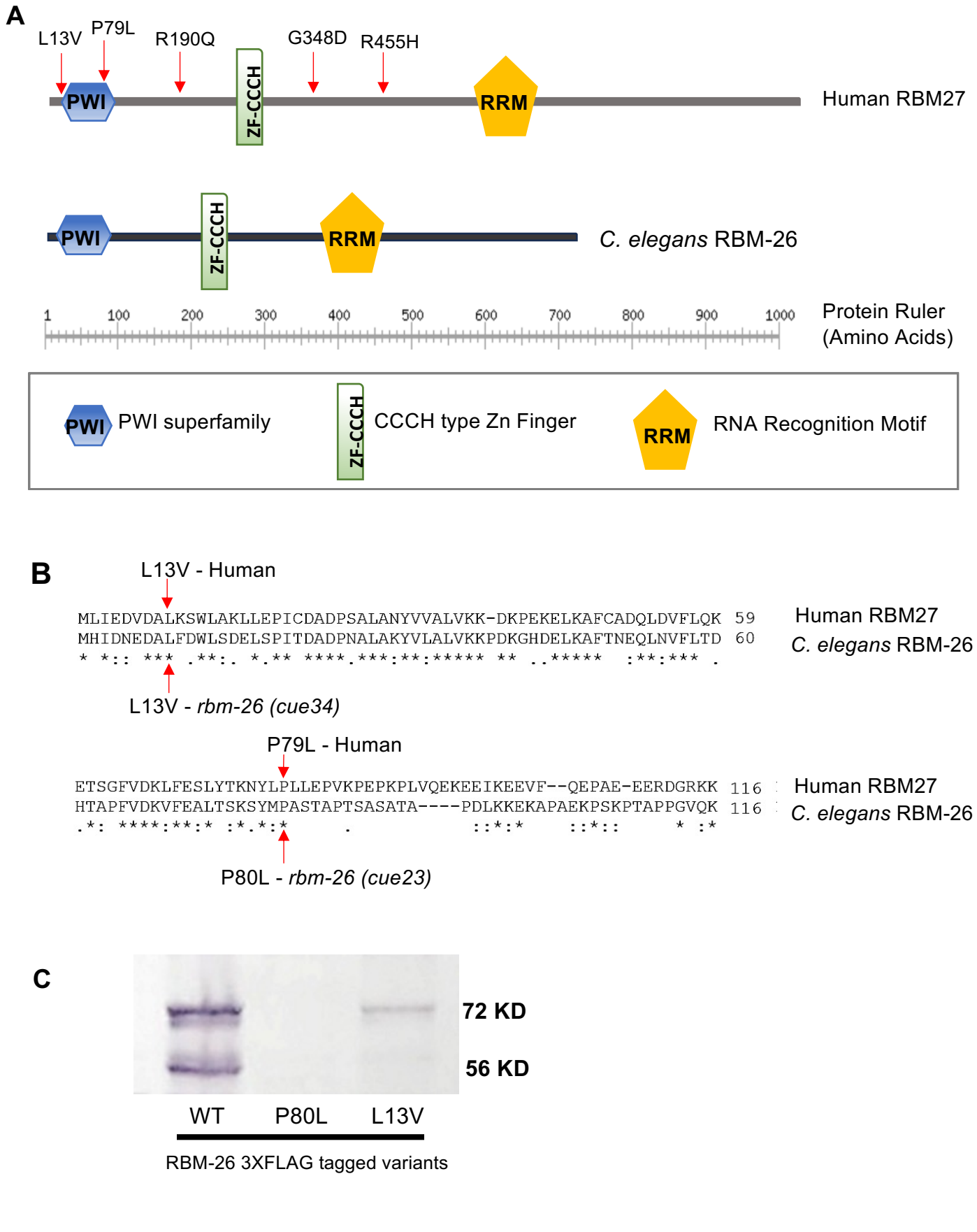
A
L13V
P79L
R190Q
G348D
R455H
PWI
ZF-CCCH
RRM
Human RBM27
PWI
ZF-CCCH
RRM
C. elegans RBM-26
1 100 200 300 400 500 600 700 800 900 1000
Protein Ruler
(Amino Acids)
PWI PWI superfamily
ZF-CCCH CCCH type Zn Finger
RRM RNA Recognition Motif
B
L13V - Human
MLIEDVDALKSWLAKLLEPICDADPSALANYVVALVKK-DKPEKELKAFCADQLDVFLQK 59
MHIDNEDALFDWLSDELSPITDADPNALAKYVLALVKKPDKGHDELKAFTNEQLNVFLTD 60
* *:: *** .**:. *.** ****.***:**:***** ** ..***** :**:*** .
Human RBM27
C. elegans RBM-26
L13V - rbm-26 (cue34)
P79L - Human
ETSGFVDKLFESLYTKNYLPLLEPVKPEPKPLVQEKEEIKEEVF--QEPAE-EERDGRKK 116
HTAPFVDKVFEALTSKSYMPASTAPTSASATA----PDLKKEKAPAEKPSKPTAPPGVQK 116
.*: ****:**:* :*.*:* . ::*:* ::*:: * :*
Human RBM27
C. elegans RBM-26
P80L - rbm-26 (cue23)
C
72 KD
56 KD
WT
P80L
L13V
RBM-26 3XFLAG tagged variants

Figure 1

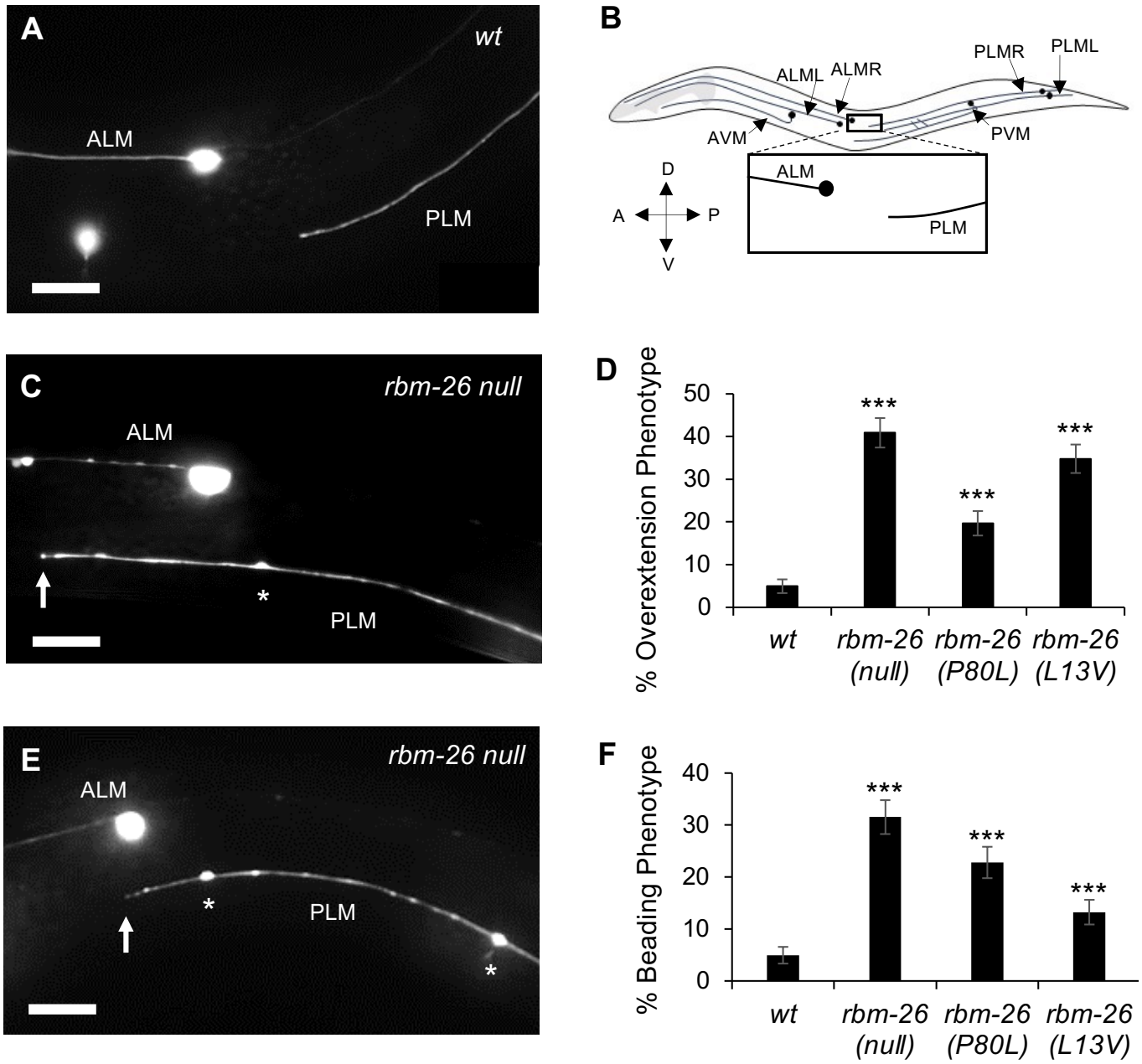
A
wt
ALM
PLM
B
ALML
ALMR
PLMR
PLML
AVM
PVM
D
A
P
V
ALM
PLM
C
rbm-26 null
ALM
*
PLM
D
% Overextension Phenotype
50
40
30
20
10
0
***
***
***
wt
rbm-26 (null)
rbm-26 (P80L)
rbm-26 (L13V)
E
rbm-26 null
ALM
*
PLM
*
F
% Beading Phenotype
40
30
20
10
0
***
***
***
wt
rbm-26 (null)
rbm-26 (P80L)
rbm-26 (L13V)

Figure 2

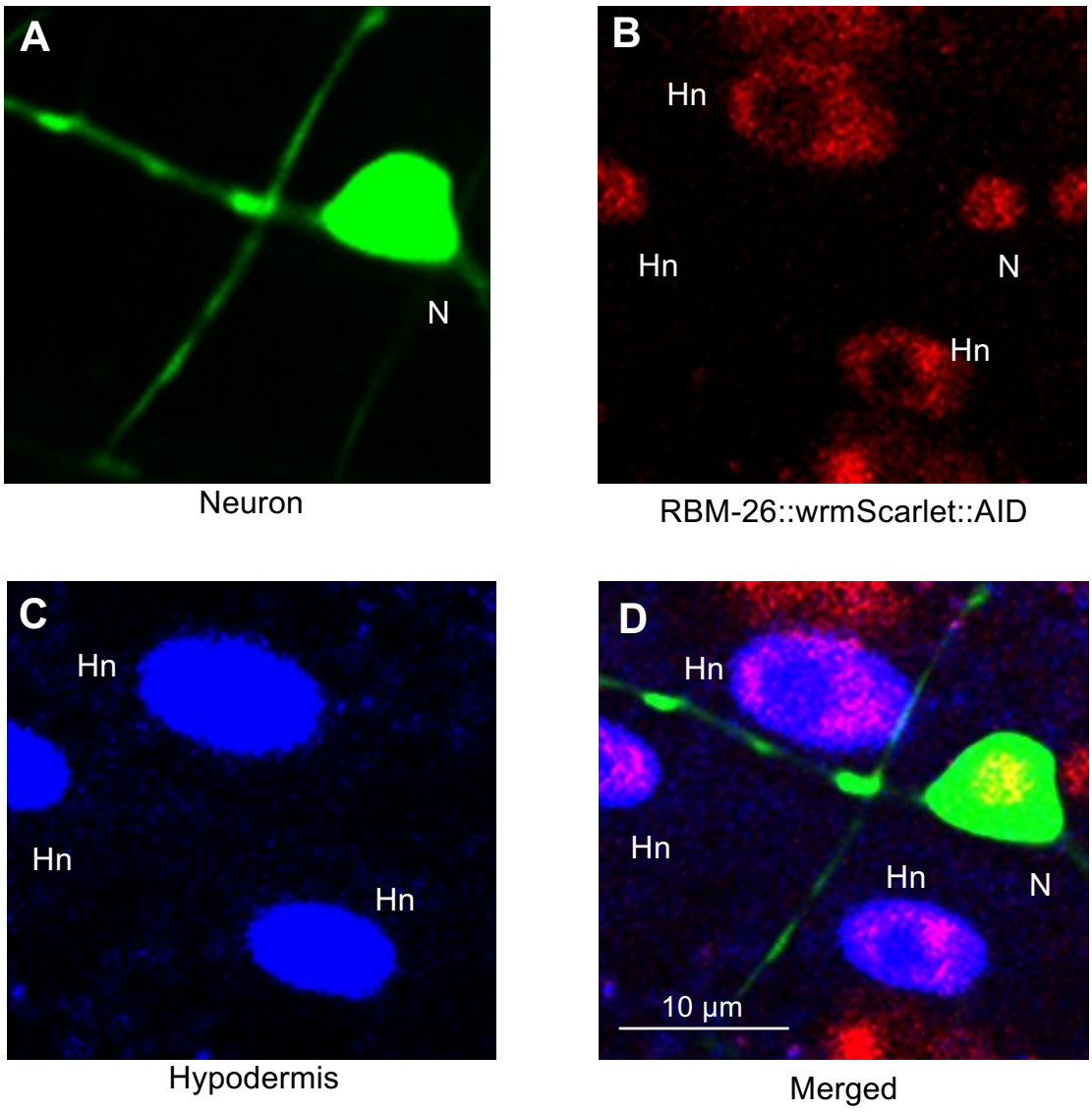
A
N
Neuron
B
Hn
Hn
N
Hn
RBM-26::wrmScarlet::AID
C
Hn
Hn
Hn
Hypodermis
D
Hn
Hn
Hn
N
10 µm
Merged

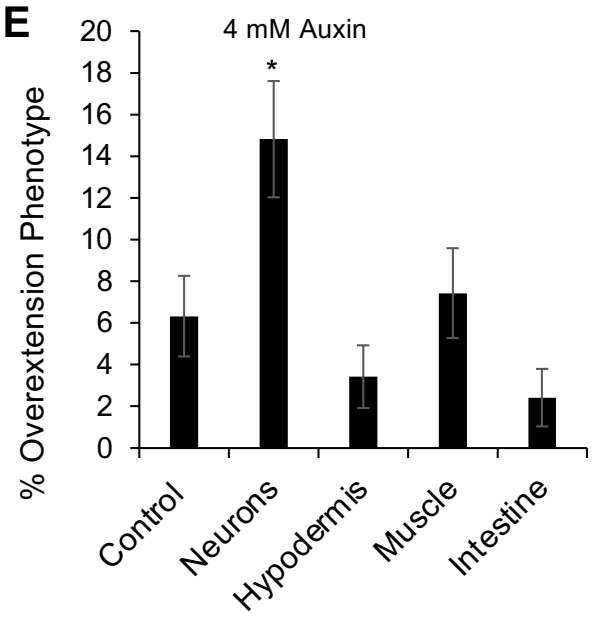
E
4 mM Auxin
% Overextension Phenotype
0
2
4
6
8
10
12
14
16
18
20
*
Control
Neurons
Hypodermis
Muscle
Intestine

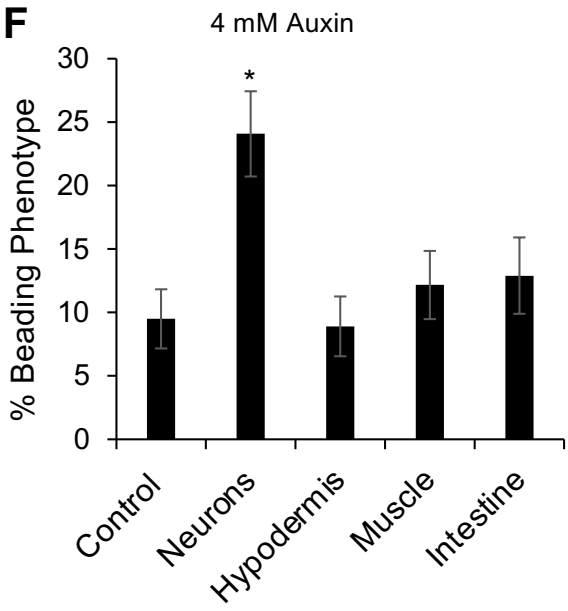
F
4 mM Auxin
% Beading Phenotype
0
5
10
15
20
25
30
*
Control
Neurons
Hypodermis
Muscle
Intestine

Figure 3

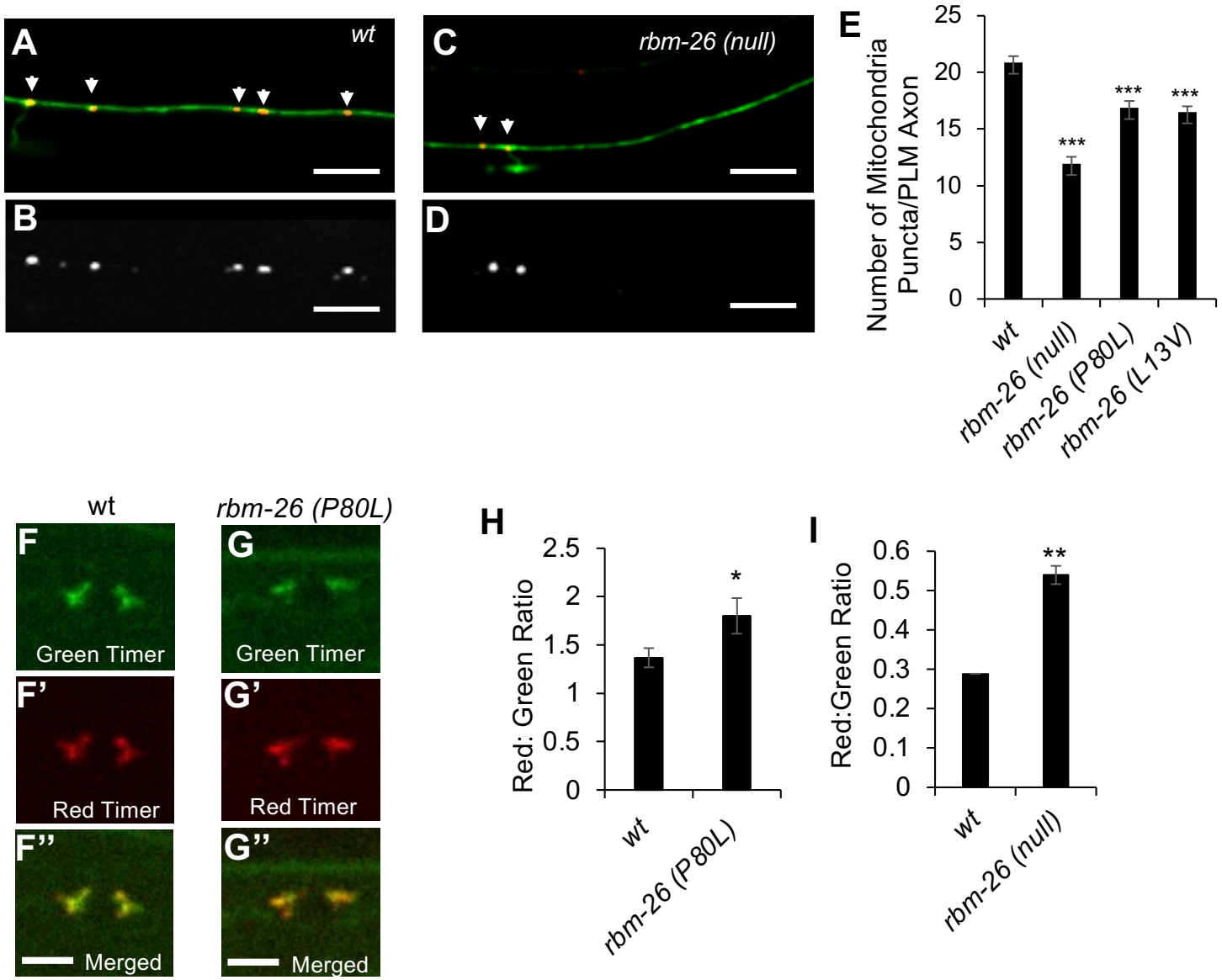
A
wt
B
C
rbm-26 (null)
D
E
Number of Mitochondria Puncta/PLM Axon
25
20
15
10
5
0
***
***
***
wt
rbm-26 (null)
rbm-26 (P80L)
rbm-26 (L13V)
wt
rbm-26 (P80L)
F
Green Timer
F'
Red Timer
F''
Merged
G
Green Timer
G'
Red Timer
G''
Merged
H
Red: Green Ratio
2.5
2
1.5
1
0.5
0
*
wt
rbm-26 (P80L)
I
Red:Green Ratio
0.6
0.5
0.4
0.3
0.2
0.1
0
**
wt
rbm-26 (null)

Figure 4

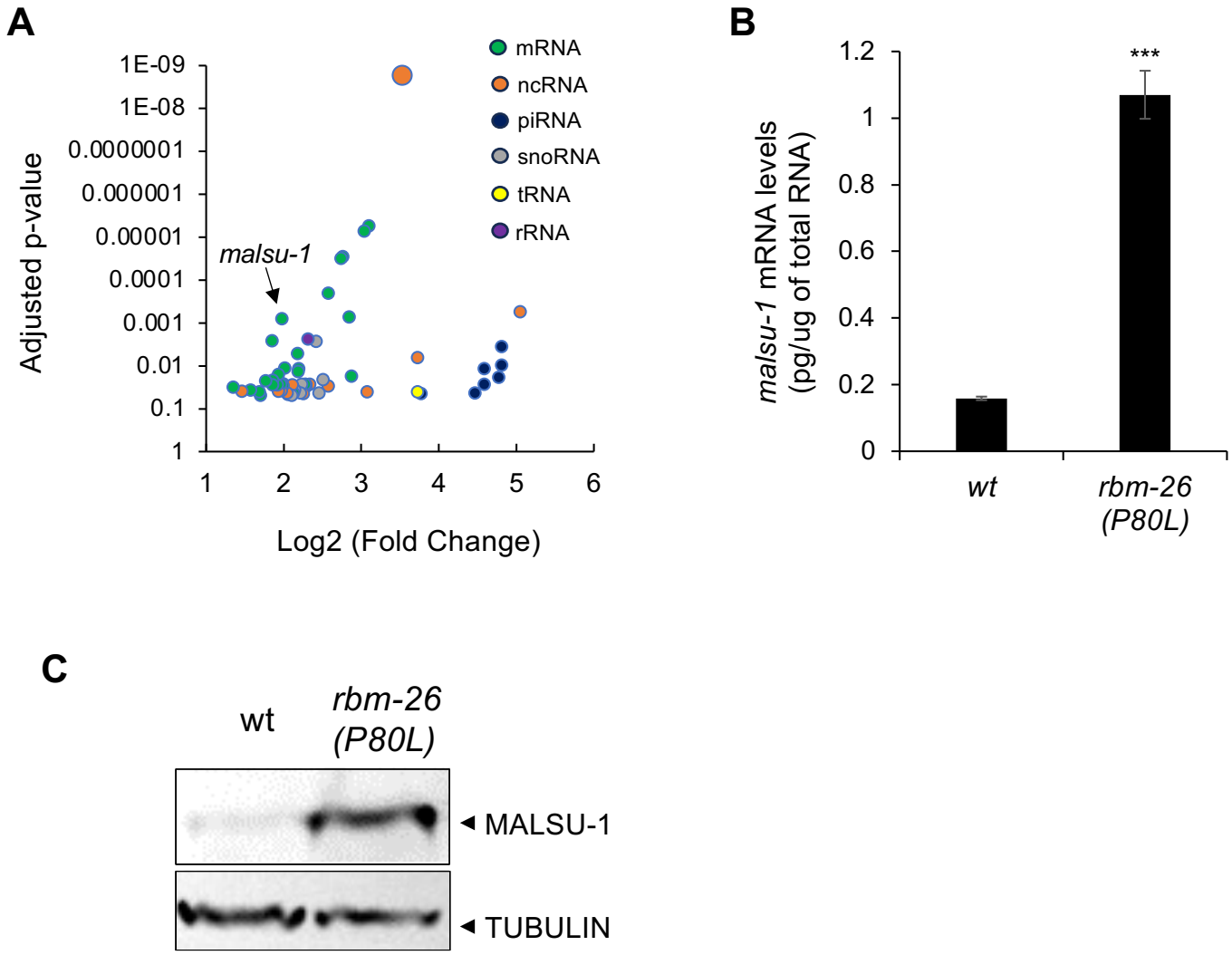
A
mRNA
ncRNA
piRNA
snoRNA
tRNA
rRNA
malsu-1
Adjusted p-value
1E-09
1E-08
0.0000001
0.000001
0.00001
0.0001
0.001
0.01
0.1
1
1
2
3
4
5
6
Log2 (Fold Change)
B
malsu-1 mRNA levels (pg/ug of total RNA)
1.2
1
0.8
0.6
0.4
0.2
0
***
wt
rbm-26 (P80L)
C
wt
rbm-26 (P80L)
MALSU-1
TUBULIN

Figure 5

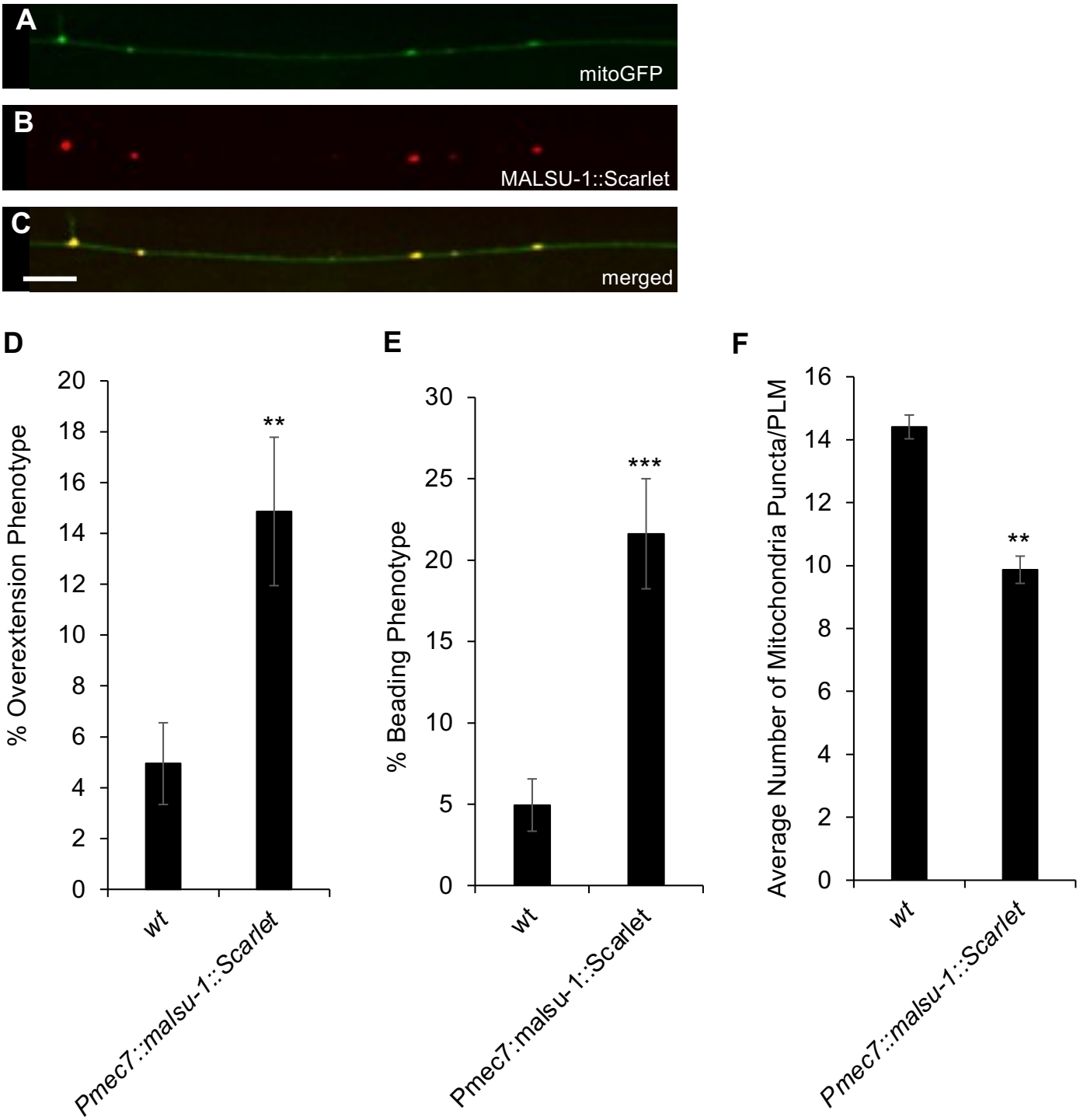
A
mitoGFP
B
MALSU-1::Scarlet
C
merged
D
% Overextension Phenotype
20
18
16
14
12
10
8
6
4
2
0
**
wt
Pmec7::malsu-1::Scarlet
E
% Beading Phenotype
30
25
20
15
10
5
0
***
wt
Pmec7::malsu-1::Scarlet
F
Average Number of Mitochondria Puncta/PLM
16
14
12
10
8
6
4
2
0
**
wt
Pmec7::malsu-1::Scarlet

Figure 6

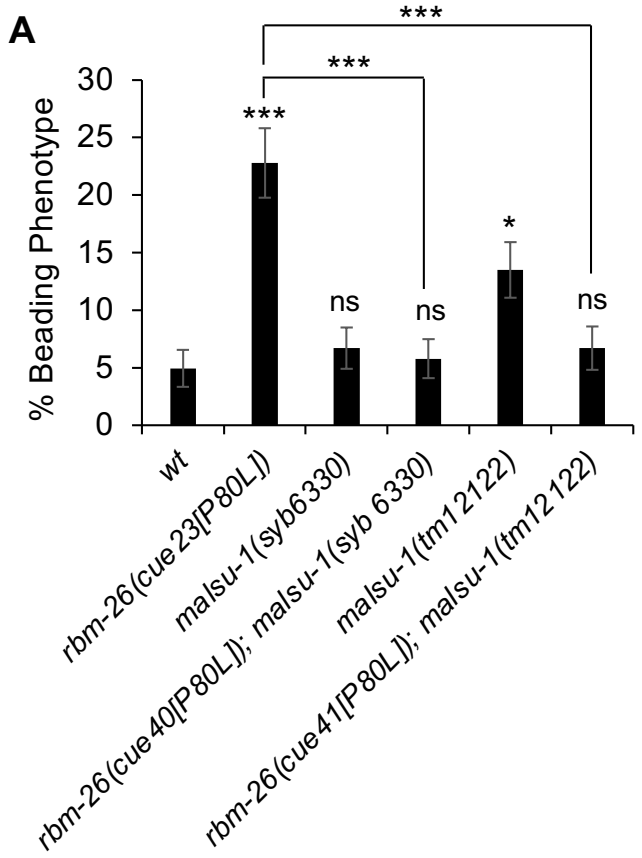
A
% Beading Phenotype
30
25
20
15
10
5
0
***
***
***
ns
ns
*
ns
wt
rbm-26(cue23[P80L])
malsu-1(syb6330)
rbm-26(cue40[P80L]); malsu-1(syb 6330)
malsu-1(tm12122)
rbm-26(cue41[P80L]); malsu-1(tm12122)

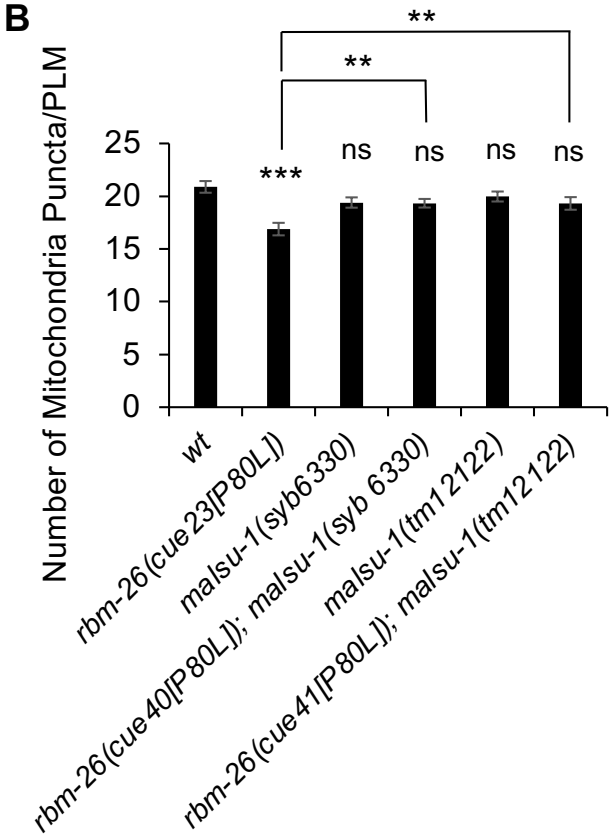
B
Number of Mitochondria Puncta/PLM
25
20
15
10
5
0
**
**
***
ns
ns
ns
ns
wt
rbm-26(cue23[P80L])
malsu-1(syb6330)
rbm-26(cue40[P80L]); malsu-1(syb 6330)
malsu-1(tm12122)
rbm-26(cue41[P80L]); malsu-1(tm12122)

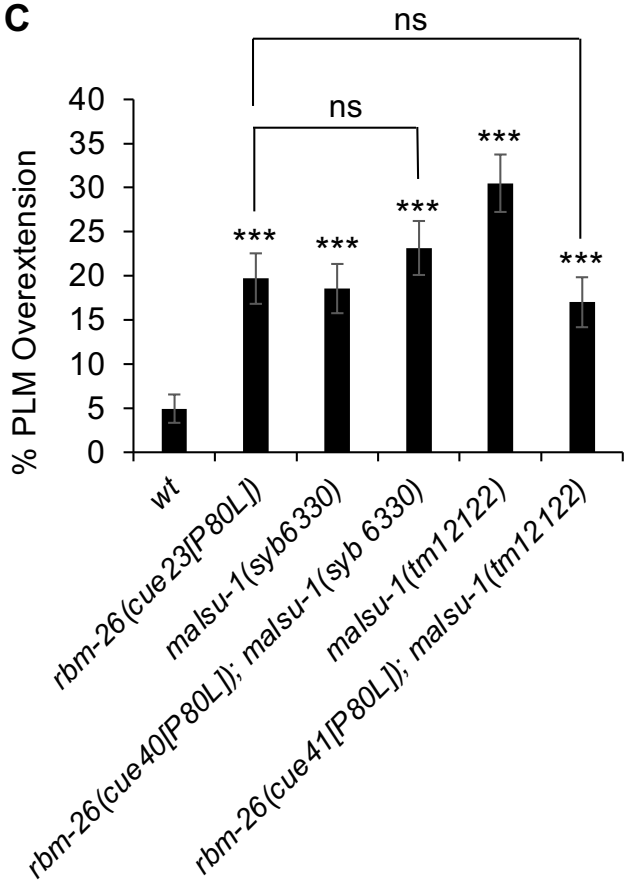
C
% PLM Overextension
40
35
30
25
20
15
10
5
0
ns
ns
***
***
***
***
***
wt
rbm-26(cue23[P80L])
malsu-1(syb6330)
rbm-26(cue40[P80L]); malsu-1(syb 6330)
malsu-1(tm12122)
rbm-26(cue41[P80L]); malsu-1(tm12122)

Figure 7

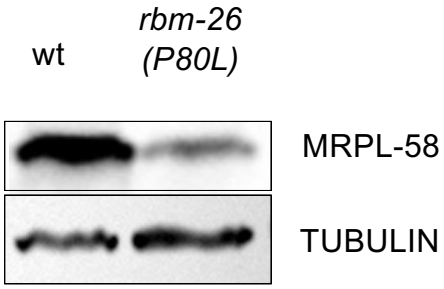

Figure 8